nature communications

Article

https://doi.org/10.1038/s41467-025-57649-1

Dynamic multimodal information encryption combining programmable structural coloration and switchable circularly polarized luminescence

Received: 9 October 2024

Accepted: 26 February 2025

Published online: 06 March 2025

Check for updates

Zeyu Feng[1,4], Jialei Li[1,4], Peng Yang[1,2], Xiangxiang Xu[1], Di Wang[1], Jiahe Li[1], Chutian Zhang[1], Jingguo Li[3], Hongli Zhang[1] ✉, Gang Zou[1,2] ✉ & Xin Chen[2] ✉

Multimodal optical-materials are highly desirable due to their advantages in enhancing information security, though independent modulation is challenging, especially accurately controlling the orthogonal relationship between the structural coloration (SC) and fluorescence (FL) pattern. Herein, we report a strategy which combines programmable structural coloration and switchable circularly polarized luminescence (CPL) for multimodal information encryption. Using photomask with aligned grating, programmable periodic patterns are fabricated on a polydiacetylene (PDA) gel film, which produces image in tunable structural colors. Introducing a chiral fluorescence layer containing perovskite nanocrystals and twisted-stacking Ag nanowires (NWs) bilayers, which provides stimuli-responsive FL and CPL with high dissymmetry factor (g_{lum}, up to 1.3). Importantly, the structural coloration information and FL patterns (including CPL pattern) can be independently modulated without mutual interference, even selectively concealed or exposed by varying microstructure design of the cross-linked PDA gel or by acetonitrile treatment.

Information storage and security have always been the perennial hot issues in society[1–3]. In the past decades, significant efforts have been made to develop anti-counterfeiting systems capable of displaying diverse information across distinct optical channels (e.g., reflection, transmittance, fluorescence (FL), and so on)[4–6]. Among them, structural coloration (SC) materials, renowned for their ability to generate color via periodic micro- and nano-structures rather than chemical pigments, have attracted enormous attention due to their ability to manipulate the flow of light as well as their prospective applications in sensors, displays, anti-counterfeiting and information encryption[7–10]. However, these reflective structural colors are only available within a limited range of observation angles and perform poorly when the ambient light is weak, hindering their applications. On the other hand, the popular FL materials in most anti-counterfeiting systems, only generate FL signals upon excitation, but often inactive under natural light[1]. Extensive studies in this field are mainly about organic dyes and dye-doped polymers, quantum dots, aggregation-induced emission molecules, and metallic complexes[11–13]. The point is that FL patterns can be easily mimicked by materials with similar FL colors, diminishing their information security[14]. Recently, circularly polarized luminescence (CPL) materials have gained considerable interest due to their inherent chiroptical information dimension and potential applications

[1]State Key Laboratory of Precision and Intelligent Chemistry, School of Chemistry and Materials Science, University of Science and Technology of China, Hefei, Anhui, China. [2]Suzhou Laboratory, Suzhou, Jiangsu, China. [3]CAS Key Laboratory of Urban Pollutant Conversion, Department of Environmental Science and Engineering, University of Science and Technology of China, Hefei, China. [4]These authors contributed equally: Zeyu Feng, Jialei Li.
✉e-mail: zhl1992@ustc.edu.cn; gangzou@ustc.edu.cn; mail.xinchen@gmail.com

in information encryption[15,16]. Great efforts have been made to amplify the high dissymmetry factor (g_{lum}) value via various strategies, including supramolecular self-assembly[17,18], aggregation-induced emission[19,20], incorporating into chiral liquid crystals system and so on[21]. The obtained g_{lum} for the most CPL-active materials is still very low (10^{-4}–10^{-2}), limiting their practical applications. To further amplify the g-factors, Professor Zhu and colleagues developed CPL materials with a high g_{lum} up to 1.9 by integrating perovskite nanocrystals (NCs) into a chiral liquid crystal system[22]. Nevertheless, the visualization of dynamic CPL patterns in higher-level anti-counterfeiting applications still remains challenging.

Compared with conventional anti-counterfeiting technique using only SC, FL, or CPL, dual or even multi-optical mode materials can greatly increase the capacity of the information storage and enhance the anti-counterfeiting level of the security labels[23]. Currently, various dual-mode or multi-mode anti-counterfeiting materials have been developed, including the combination of structural color and fluorescent[24], fluorescent patterns with surface wrinkles[5] or cooperated with phosphorescence[25], and so on. Yu et al. designed dual-mode geminate labels by programming fluorescent cholesteric liquid crystal microdroplets, combining both reflective and fluorescent patterns[26]. Wu et al. demonstrated the fabrication of dual-mode patterns on an azopolymer via orthogonal photopatterning technique[27]. However, the limitation for the current dual or multi-optical mode materials lies in their inability to independently modulate SC, FL, and CPL information, and their insufficient stimulus responsiveness[14]. In addition, two different optical mode patterns in the same region (e.g., SC and FL information) often suffer from strong mutual interference during fabrication and usage, especially during the dynamic regulation process. In this regard, it remains a great interest to develop anti-counterfeiting materials with independently programmable structure color, stimulus-responsive FL, and CPL performance, which is crucial for dynamic multimodal information encryption.

Herein, we reported a strategy to fabricate multimodal dynamic information anti-counterfeiting system that combines programmable SC, switchable FL, and CPL. Two-dimension (2D) programmable photonic patterns could be fabricated on a diacetylene organogel film via multi-stage photo-patterning process. The SC information, including color gamut and patterns, could be tunned easily by varying the direction of incident light or by acetonitrile (ACN) treatment. Achiral perovskite NCs were employed as FL emission primitive due to their ease of fabrication and greater tunability[28]. By the integration of twisted-stacking Ag nanowires (NWs) bilayers, the hybrid films exhibited CPL signal, favoring for the circular polarization-selective image discrimination with the naked eye. The FL and CPL patterns (including color and handedness direction) could further be modulated by halogen anion exchange of the perovskite NCs. The SC information and FL (including CPL) patterns could be independently modulated without mutual interference during the dynamic regulation process. Moreover, through periodic structural design for the cross-linked polydiacetylene (PDA) gel film, the SC information and FL even CPL patterns could be selectively concealed or exposed, allowing for multistage secure information encryption and programmable decryption. Compared to the traditional multi-mode anti-counterfeiting systems, our proposed strategy possesses several significant features. First, the prepared hybrid films exhibited high CPL performance ($g_{lum} > 1$), favoring the circular polarization-selective image discrimination with the naked eye, which would further enrich the library of multi-mode and multi-level anti-counterfeiting systems. Second, the dynamic modulation of both SC and FL/CPL information could be easily achieved independently, greatly enhancing the information capacity and increasing security levels in anti-counterfeiting systems. Third, based on periodic structure design, the SC and FL/CPL information could be selectively concealed or exposed, allowing for multistage secure information encryption and programmable decryption.

Results

Designing strategy

Figure 1 illustrates our overall strategy to achieve dynamic multimodal information Encryption combining programmable SC, tunable FL, and CPL characteristics. The top PDA microarrays with 2D programmable photonic patterns were fabricated via multi-stage photo-patterning process, displaying the programmed SC information. For example, a double-periodic PDA microarrays, consisting of “elephant” pattern with vertical alignment and “panda” pattern with parallel alignment, could be successfully fabricated, which exhibited interesting SC image switching from “elephant” to “panda” upon rotating (Fig. 1a). The iridescent SC performance should obey the Bragg’s law[29]. The flexible fluorescent patterns containing perovskite NCs could be prepared via screen printing technique and twisted-stack Ag NWs bilayers were transferred onto the surface of fluorescent patterns to generate optical activity. The FL and CPL patterns (including color and handedness direction) could be modulated through the halogen anion exchange process (Fig. 1a). It should be noted here that the aspect ratio of the periodic structure of top PDA microarrays affected greatly their SC and FL/CPL performance. As shown in Fig. 1b, the encrypted SC and FL/CPL information of the hybrid films could be selectively concealed or exposed by manipulating the aspect ratio of periodic structure of the top PDA microarrays. Moreover, upon external stimuli, e.g., ACN treatment, their SC and FL/CPL performance could be further switched “on” or “off”, which also greatly depended on the periodic structure of top PDA microarrays.

2D photonic patterns in PDA organogels films

The diacetylene monomer, 2,4-hexadiyn-1,6-diacrylate, was synthesized in analogy to the previous procedure[30], and characterized with ^{1}H-NMR (Supplementary Fig. 1). After irradiation with a mercury lamp through a photomask (coupled with aligned grating) for 2 min (Fig. 2a), the unmasked section turned yellow to form gel and exhibited a broad absorption band (Supplementary Fig. 2), indicating the successful formation of the cross-linked network, as consistent with the previous report[31]. Meanwhile, two characteristic Raman vibrational bands at 2265 and 1728 cm^{-1}, were observed (Supplementary Fig. 3), corresponding to the C≡C and C=C stretching vibrations in the PDA backbone. Upon UV irradiation through the photomasks (coupled with aligned grating), PDA gel with the designed pattern could be prepared via a photo-polymerization process, which was determined by the photomask. While the inherent periodic structure of PDA microarrays within the patterns was determined by the aligned grating. The scanning electron microscope (SEM) characterizations indicated the successful fabrication of uniform PDA cuboid microarrays (10 μm in length and 1 μm in width) on the substant of glass (Supplementary Fig. 4). The patterned PDA film exhibited angle-dependent iridescent SC by varying viewing angles, α or the direction of incident light, β (Fig. 2b, c and Supplementary Fig. 5). For instance, the pattern of a “penguin” was recorded that showed distinct colors from different viewing angles due to wavelength-dependent diffraction (Fig. 2d). In addition, by varying the direction of incident light, the displayed “penguin” image can be reversibly switched on and off in selective areas duo to the inherent double periodic structure within the cuboid microarray (10 μm in horizontal spacing and 1 μm in vertical spacing). Basically, structural colors were visible when the direction of incident light was parallel to that of the periodicity and could be reversibly switched by varying the direction of incident light. As mentioned above, the direction of the aligned cuboid microarrays was determined by the direction of aligned grating structure of the photomask. A complexed “USTC” pattern could be created with varying directions of the aligned cuboid microarrays through a multistage photo-patterning process (Supplementary Fig. 6). Therefore, isolated “U”, “S”, “T” and “C” rainbow characters can be selectively read out by tuning the direction of incident light, since they were visible on one side only

https://doi.org/10.1038/s41467-025-57649-1

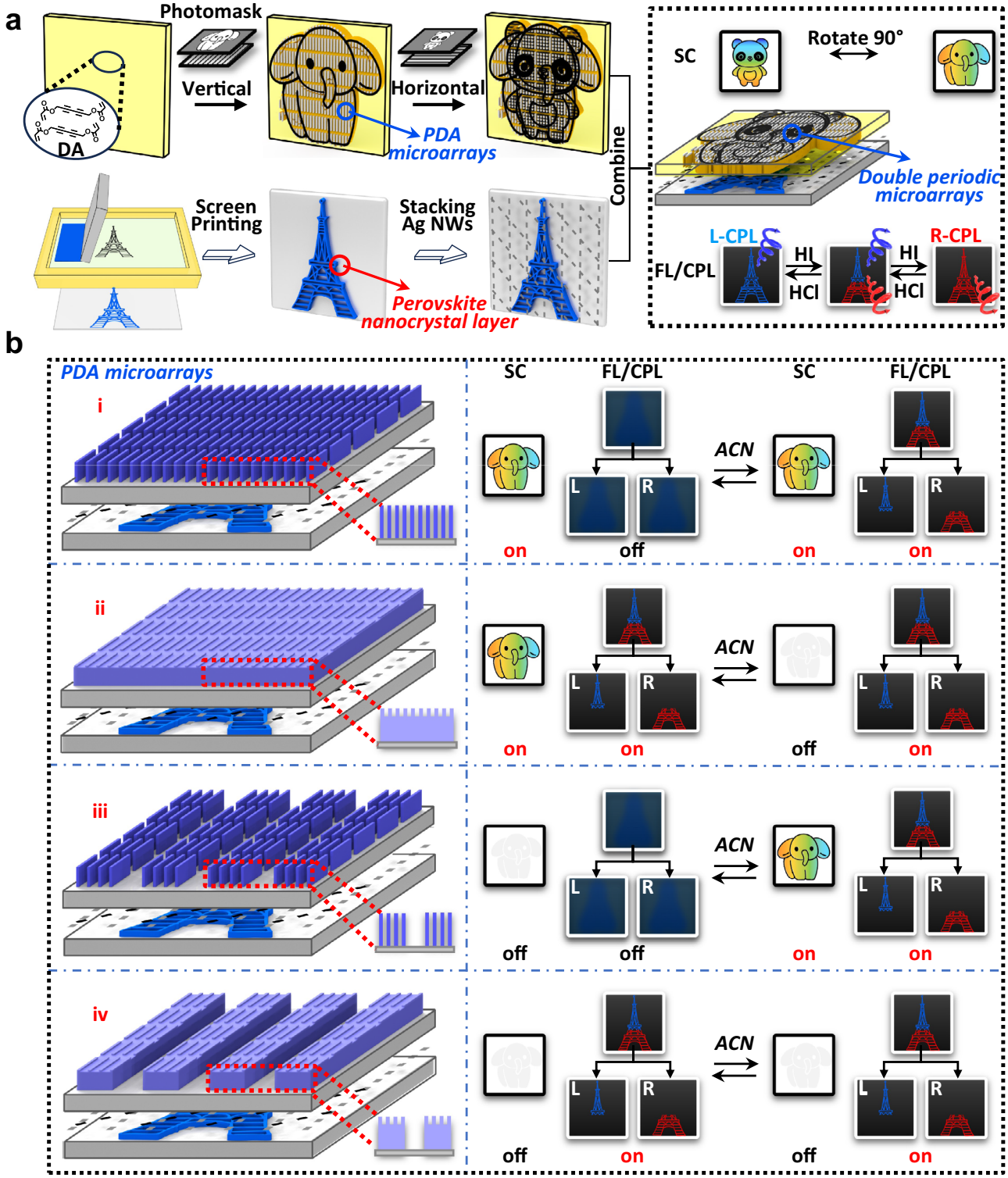

Fig. 1 | Design strategy of a multimodal dynamic information encryption system. a Illustration of the fabrication process: the top PDA microarrays with 2D programmable photonic patterns were fabricated via multi-stage photo-patterning process; and the bottom flexible FL patterns layer containing perovskite nanocrystals were fabricated via screen printing technique and the twisted-stacking Ag NWs bilayers were further transferred onto the surface of the FL patterns layer to generate CPL signal. Their SC and FL/CPL information could be independently modulated. **b** By manipulating the aspect ratio of periodic structure of PDA microarrays or external ACN treatment, the encrypted SC and FL/CPL information could further be selectively concealed or exposed. DA diacetylene, PDA polydiacetylene, ACN acetonitrile, SC structural coloration, FL fluorescence, CPL circularly polarized luminescence.

where the direction of incident light was parallel to that of the periodicity (Fig. 2e). According to Bragg's law, their angle-dependent iridescent SC was affected by the periodic structure of PDA microarray, the direction of incident light and the viewing angle. No apparent difference in angle-dependent iridescent SC performance could be observed upon tilting (Supplementary Fig. 7). When the microarrays were prepared on a flexible substrate, like PVA, the film showed a blue shift of the colors when it was stretched perpendicular to that of the

https://doi.org/10.1038/s41467-025-57649-1

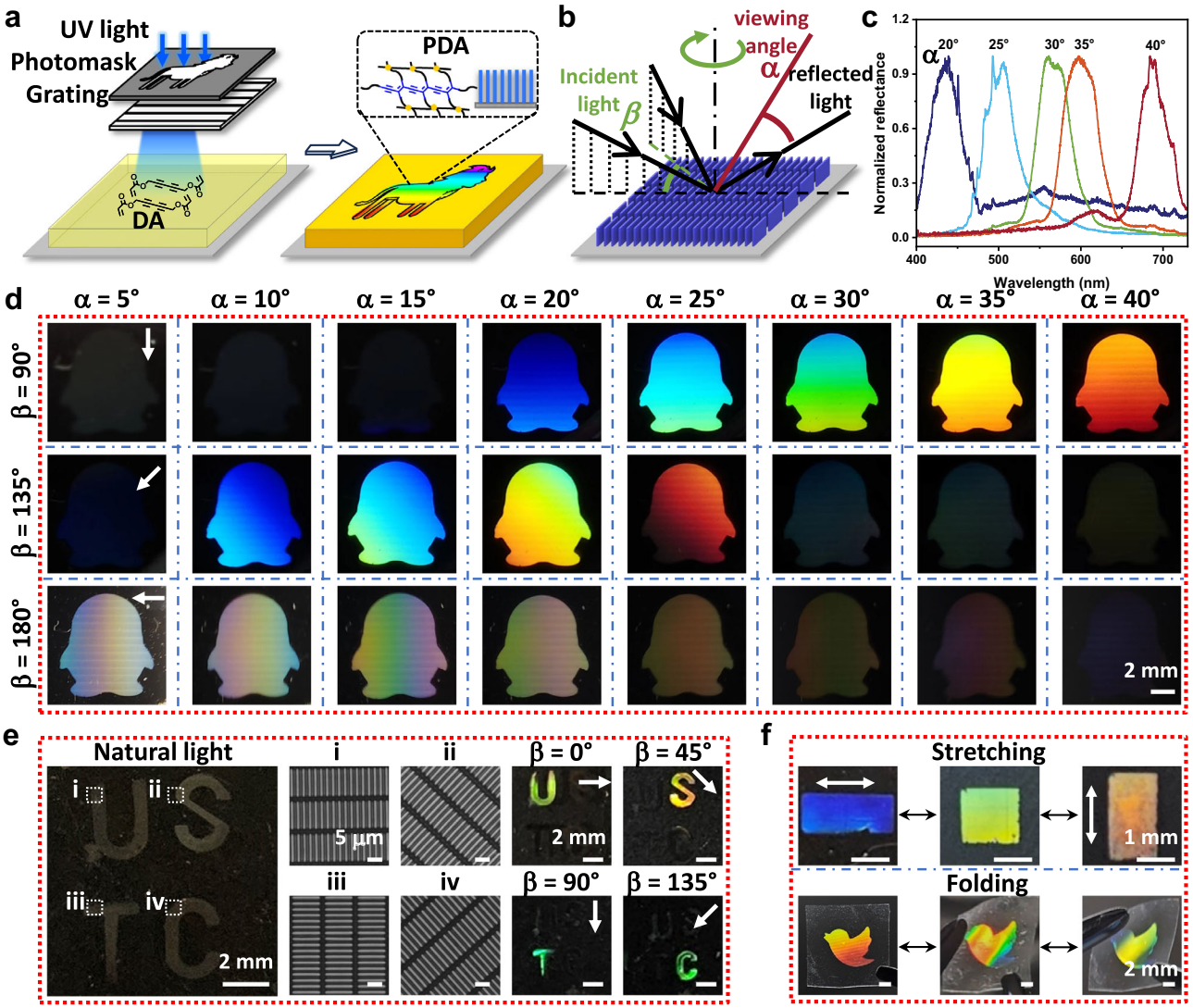

Fig. 2 | Programmable structural coloration. a Fabrication of patterned PDA microarrays. **b** PDA microarrays exhibited angle-dependent structural coloration by varying the viewing angles, α, or the direction of incident light, β. **c** Reflectance spectrum of structural coloration at varying the viewing angle α. **d** photographs of the "penguin" image at different combinations of viewing angle α and the incident angle of the incoming light, β. **e** A "USTC" pattern, in which each letter was created with a particular alignment of cuboid microarrays and showed a particular structural coloration observable only when illuminated with light with a particular incident angle. **f** Changes of structural coloration of the flexible PDA microarrays upon stretching or folding.

periodicity of the microarrays, due to the decrease of the periodic spacing. On the contrary, the film exhibited a red shift of the colors when it was stretched parallel to that of the periodicity, as a result of increased periodic spacing (Fig. 2f and Supplementary Fig. 8). The exhibited structure colors also varied upon folding, extending their potential for portable information encryption and anti-counterfeiting systems.

In principle, the SC greatly depended on not only the view angle but also the periodic nanostructures[32]. Therefore, we anticipate that the structural colors could be fine-tuned by varying the periodicity of the PDA microstructure. In this work, four kinds of 2D periodic structure of PDA cuboid microarrays were fabricated by a multistage photopatterning process (see experimental section for details), as outlined in Supplementary Fig. 9. Firstly, after irradiation with a mercury lamp through a photomask with the aligned grating structure for 2 min, 2D periodic structure of the cuboid microarray of PDA with 1.5 μm in thickness (structure "i", Fig. 3a, Supplementary Figs. 10a and 11a) could be fabricated. Then UV irradiation from back would further induce the photopolymerization of the unreacted DA monomer within the region between the adjacent the cuboid. Therefore, 2D periodic structure of PDA cuboid microarray with 80 nm in thickness (structure "ii", Fig. 3b and Supplementary Figs. 10b and 11b) could be prepared. By combining with an aligned grating structure (60 μm in spacing), 2D periodic structure of the cuboid microarray of PDA with 1.5 μm or 80 nm in thickness (structure "iii", Fig. 3c and Supplementary Fig. 10c; structure "iv", Fig. 3d and Supplementary Fig. 10d) could be fabricated respectively by a similar two-step photopatterning process. As expected, above four kinds of 2D periodic structure of PDA cuboid microarray indeed exhibited different structure colors performance (Fig. 3). In the case of structure "i", the fresh prepared films exhibited rainbow image of "A". Upon treatment with ACN, no obvious SC changes could be observed (Fig. 3a), since the gap of the periodic microstructure could not be fully filled with due to its own higher aspect ratio and surface tension of ACN. In contrast, for structure "ii", the SC pattern disappeared upon ACN treatment (Fig. 3b). This is related to the low aspect ratio of the structure "ii", which allows the easy penetration of ACN into the interior of the PDA microarray, resulting the change in the refractive index contrast and spectral reflectance (Supplementary Fig. 12b). It is worth mentioning that the structural change is reversible upon removal of ACN, which is further supported by recovery of SC. In

https://doi.org/10.1038/s41467-025-57649-1

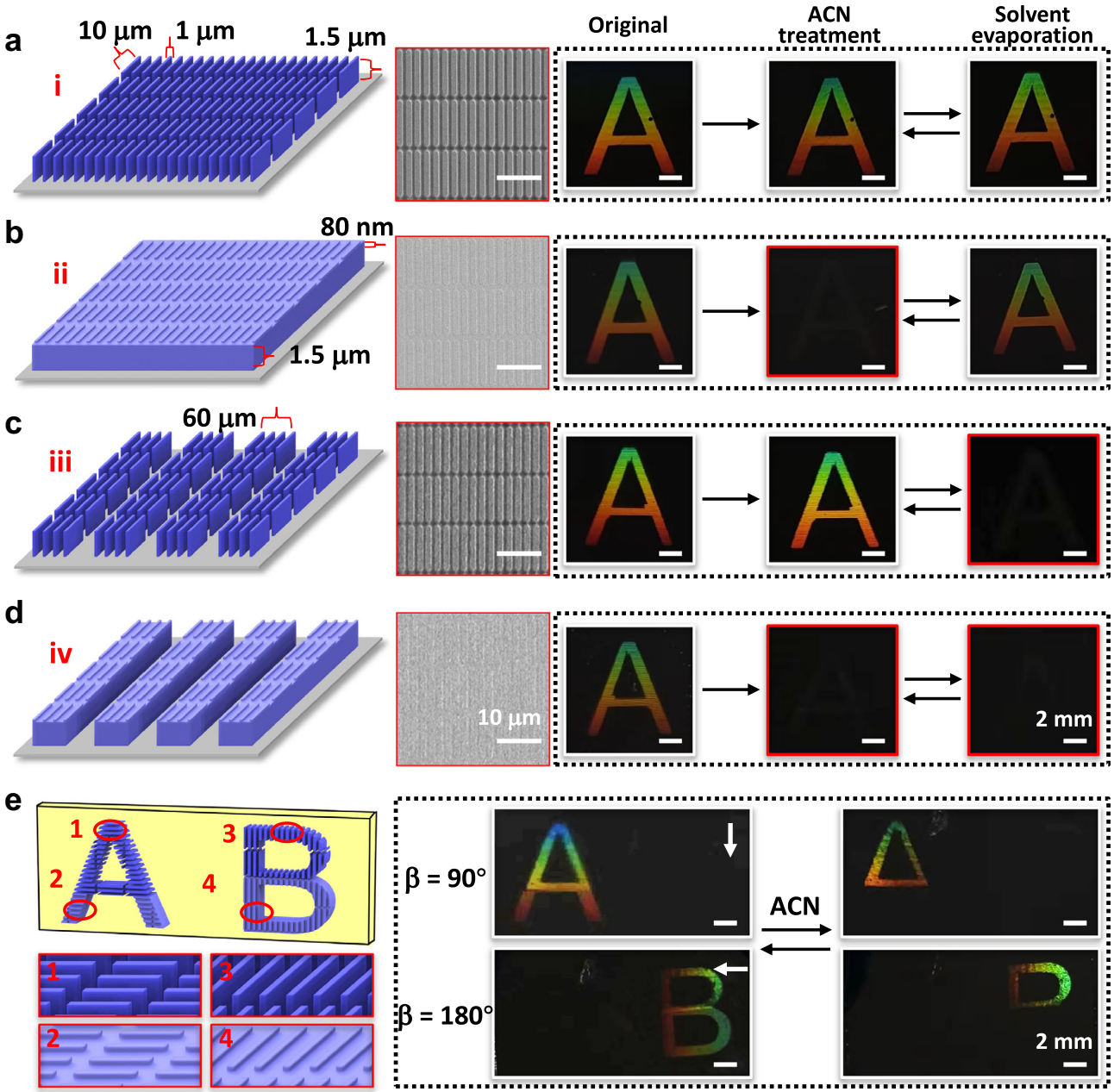

Fig. 3 | Dynamic structural coloration of periodic structure of the patterned PDA microarray. a–**d** show four typical micropatterns, as well as their corresponding Scanning electron microscope (SEM) characterizations and structural coloration change when treated with ACN. **e** The complexed "AB" pattern was generated by combining cuboid microarray structures "**i**" and "**ii**" in different aligned directions, resulting in distinct structural coloration performance upon varying incident light directions or ACN treatment.

the case of structure "iii", the fresh prepared films exhibited rainbow image of "A". Upon treatment with ACN, no obvious structure and SC changes could be observed, similar as that of structure "i". After remove of ACN, obvious in-plane shrinkage phenomenon could be observed due to the large unoccupied spacing between the adjacent PDA microarrays strips. This anisotropic and nonuniform in-plane shrinkage would disrupt the periodic structure of PDA microarrays in structure "iii", leading to the disappearance of structural color (Supplementary Fig. 12c). Interestingly, this in-plane shrinkage could be recovered upon treating with ACN again, accompanied by reversible SC expression, as shown in Fig. 3c and Supplementary Fig. 12. In the case of structure "iv", the fresh prepared films exhibited rainbow image of "A". Upon treatment with ACN, the low aspect ratio of the structure "iv" allowed the easy penetration of ACN into the interior of the PDA microarray, resulting in the change in the refractive index contrast and the disappearance of the SC (Fig. 3d). After solvent evaporation, the penetration of ACN into the interior of the PDA microarray would be removed. However, similar in-plane shrinkage occurred, leading to the destroy of the periodic structure of PDA microarrays and the disappearance of structural color (Supplementary Fig. 12d). Therefore, the SC in structure "iv" could not be recovered after removal of ACN.

By engineering the patterning protocol, different periodic microstructures could be programmed at designated regions on the same device, therefore, different SC patterns would be expected upon external stimuli. As shown in Fig. 3e, the patterned photonic structure "A" consisting of structure "i" and "ii" with the periodicity direction of 90° could be fabricated by a two-step photopatterning process. Then the patterned photonic structure "B" consisting of structure "i" and "ii"

with the periodicity direction of 180° could be fabricated in orthogonal photopatterning. "A" and "B" rainbow characters appeared alternately by varying the direction of incident light, and more importantly, their appearance could be dynamically tuned upon ACN treatment (Fig. 3e). This programmable patterning strategy could greatly enhance the capacity of information storage and promote the anti-counterfeiting level of the security labels.

Switchable FL/CPL patterns

Designing CPL-active materials with high g_{lum} value (>1), mechanical deformability and tailorable CPL characteristics for dynamic anti-counterfeiting remain challenging. Recently, twisted stacking of two or more layers of nanomaterials, e.g., Ag NWs, has emerged as a powerful strategy to introduce optical activity into achiral solid-state systems. Along this strategy, we expect that the twisted-stacked silver nanowire arrays (TNA) could be employed as optical converter for an achiral perovskite FL overlayer, to generate CPL. To test our hypothesis, a "butterfly" achiral FL pattern was screen printed using a mixture of PDMS with $CsPbCl_3$ (blue) and $CsPbI_3$ NCs (red) first. Three kinds of perovskite ($CsPbX_3$, X=Cl, Br, I) NCs were prepared, each-responsible for one of the three prime colors (blue, green, red) of FL. Their respective morphologies were observed by TEM (Supplementary Fig. 13). Then Ag NWs bilayers, with a twisted-stacking angle of 45° or −45° (Supplementary Figs. 14 and 15), were transferred onto the surface of fluorescent patterns to generate optical activity (g_{abs} up to 0.4). The chiral twisted-stacked Ag NWs bilayers could act as the circularly polarizing converter to generate CPL signal, favoring for the selected visual effect when viewed through left- or right-handed circularly polarizing filters (CPF), as outlined in Fig. 4a. The TNA have strong CD absorptions, a positive and a negative absorption at around 420 and 700 nm due to Cotton effect (Supplementary Fig. 16), suggesting their frequency dependence optical activity and could be exploited as circular polarization-based converter to generate CPL. Besides, CPL characterization was conducted by rotating the sample around the normal axis of the hybrid films to investigate the potential effect of linear dichroism. The variation in CPL signal intensities across all rotation angles was found to be insignificant when compared to the prominent CPL signals, thereby confirming that the primary contribution of the CPL signals came from the genuine chiroptical effects intrinsic to the twisted-stacking structure of Ag NWs, rather than solely from linear polarization effect (Supplementary Fig. 17).

For instance, the TNA films with a twisted-stacking angle of 45°, more left-handed blue CPL got transmitted and casted a blue pattern when viewed with left-handed CPF. On the other hand, right-handed red CPL was more transmissive through TNA films with twisted-stacking angle of 45°, and red pattern was received when viewed with right-handed CPF. Essentially, through selecting left- or right-handed CPF, it is possible to display either the blue wing or the red wing (Fig. 4b). Interestingly, under unpolarized UV irradiation, the "butterfly" with both blue and red wings could be observed by the naked eye. Moreover, the magnitude and handedness of CPL could be gradually tuned by varying the twist angle between TNA structures. As shown in Fig. 4c, when the twist angle varied from 45° to 0° and finally to −45°, the corresponding positive blue CPL signals gradually decreased to zero and finally became negative. On the contrary, negative red CPL signals gradually increased to zero and finally became positive upon varying the twist angle from 45° to −45°, while spectral shape remained almost the same (Fig. 4d). The thickness of twisted-stacked Ag NWs bilayers played an important role in their CPL performance. Firstly, the thickness of top Ag NWs layer (as the phase retarder) was fixed to be about 160 nm, and the luminescence asymmetry coefficient was characterized in detail by varying the thickness of the bottom Ag NWs layer (as the polarizer). As shown in Supplementary Fig. 18a, the observed g_{lum} value increased with increasing the thickness of the bottom Ag NWs layer, since thick polarizer is conductive to produce linear polarized luminescence. when the thickness of bottom Ag NWs layer reached about 600 nm, the observed g_{lum} value gradually saturated. Then the thickness of bottom Ag NWs layer was fixed to be about 600 nm, and we studied their CPL performance by varying the thickness of top Ag NWs layer. As shown in Supplementary Fig. 18b, the observed g_{lum} value decreased with increasing the thickness of top Ag NWs layer, since the phase difference is greatly related to the thickness of the phase retarder layer[33]. Very importantly, the luminescence asymmetry factor could reach as high as ±1.3 by adjusting the thickness and optical activity of TNA films (Fig. 4e), much higher than most reported perovskite-based CPL materials[15]. Five hybrid films were prepared in different batches, and showed good reproducibility, which was calculated to have a relative standard deviation (RSD) of 3.4% (Supplementary Fig. 19a). To further investigate the uniform of the twisted stacking Ag NWs bilayer on $CsPbX_3$ perovskites doped PDMS surface, we investigate the CPL performance at 9 different regions within the hybrid films. CPL intensities at different regions were marginal compared with the intense CPL signals (RSD = 2.0%), indicating the uniform of the hybrid film across a large area (Supplementary Fig. 19b). Apparently, CPL signals of the hybrid films onto curved substrates (diameters $D = 2$ cm) were virtually indistinguishable, indicating that bending of the films hardly affected their CPL performance. Moreover, the hybrid films exhibited excellent stability upon mechanical stress (about 50 N, Supplementary Fig. 20). Furthermore, the obtained g_{lum} value for the hybrid films was always higher than the g_{abs} value of Ag NWs bilayers, which might be ascribed to two possible reasons. One might be attributed to the instrument difference between CD and CPL measurements. The other should be ascribed to the inherent chiral structure of twisted-stacking Ag NWs bilayers, which act as not only the role of handedness-selective filter to selectively transmits circularly polarized luminescence with one handedness, but also the circularly polarized converter, further amplify the g-factor of obtained CPL. In the latter case, the bottom layer of Ag NWs could act as the polarizer to produce linear polarized luminescence, while the top Ag NWs layer could be treated as the phase retardation layer, further converting linear polarized luminescence to circularly polarized luminescence based on Jones matrices mechanism[34,35].

It should be noted that in the case of $CsPbBr_3$ NCs, only weak green CPL signal could be observed, owing to weak optical activity of TNA films at around 530 nm (Supplementary Fig. 21). The handedness of green CPL flips upon varying the twist angle from 45° to −45°, confirming that the origin of CPL should be ascribed to the overlapping between the emission of NCs and the optical activity of TNA films. In addition, the emission wavelength of NCs could be fine-tuned from 420 to 640 nm via anion exchange, apparent color variation could be observed (Supplementary Fig. 22), consistent with CPL and FL spectra (Fig. 4f). It is worth noting that the treatment with ammonia gas could enhance the FL intensity and the corresponding CPL performance since ammonia gas could effectively passivate surface defects of NCs[36] (Supplementary Fig. 23). All above results indicated that the magnitude, handedness, and color of CPL could be well-tuned by modulating the twist angle, the type of anions in NCs and chemical treatment.

Moreover, the hybrid films exhibited thermal sensitivity, which could be utilized as intelligent sensing labels for enhancing the security of the encrypted information or monitoring the cold-chain transport process. As shown in Supplementary Fig. 24, the fluorescent intensity for labels kept under 5 °C exhibited remained almost unchanged over 2 weeks while those decrease greatly in 10 min when kept at 60 °C. Clearly, this temperature-dependent FL variations in labels reflect the thermal history of the storage, which was critical for the cold-chain transport process. Moreover, the FL decreased quickly upon UV exposure, and the encrypted information would be easily destroyed after 7 min UV irradiation, which prevented possible data leakage and further enhanced the encrypted information security. Besides, the

https://doi.org/10.1038/s41467-025-57649-1

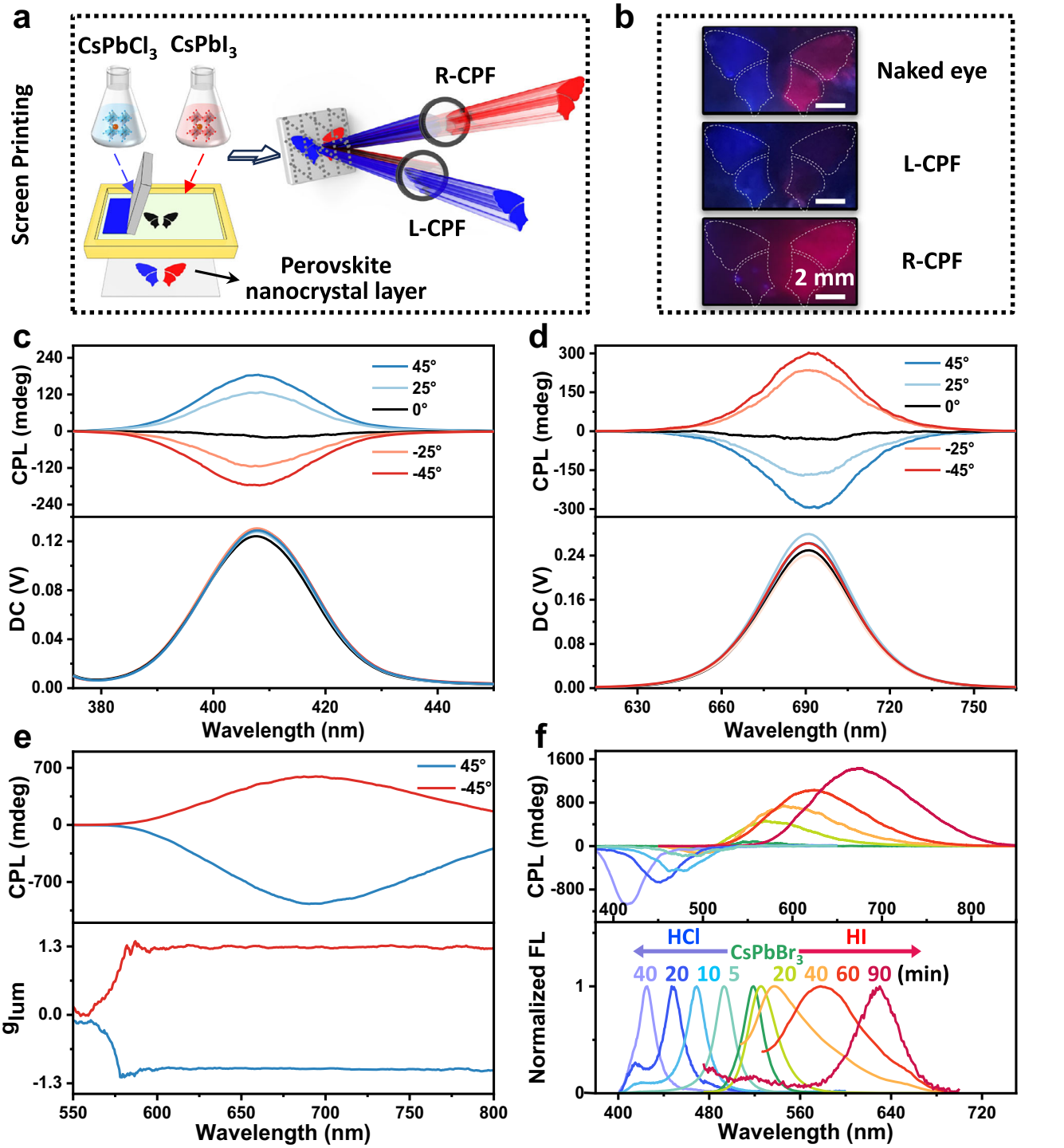

Fig. 4 | Switchable FL and CPL. a Schematic of fabricating chiral FL layers with distinguished CPL. **b** Photographs of the freshly prepared chiral "butterfly" FL pattern viewed directly by the naked eyes, or through a left or right-handed circularly polarizing filter, respectively. CPL spectra of chiral FL layer consisting of TNA structure and $CsPbCl_3$ (**c**) and $CsPbI_3$ (**d**) layer. Their CPL performance could be fine-tuned upon varying the twist angle. **e** CPL of The $CsPbI_3$/TNA hybrid films with the maximum g_{lum} value of 1.3. **f** Normalized FL spectra and the corresponding CPL upon treatment of anion exchange. CPF circularly polarizing filters.

surface coating with PDMS would greatly enhance the long-term stability of $CsPbX_3$ perovskites in water, which is crucial for real-world applications (Supplementary Fig. 25).

Design strategy of multimodal information encryption system

For multimodal information encryption systems, the mutual interference among different optical channels is always a big challenge. We therefore evaluated the impact of 2D periodic structure of PDA cuboid microarrays (type i–iv as depicted in Fig. 3) on the chiral perovskite FL layer (in the case of $CsPbBr_3$ NCs). For structure "i", both the FL intensity (Fig. 5a) and the corresponding CPL performance of the chiral perovskite FL layer significantly decreased (Supplementary Fig. 26a), owing to strong diffraction and scattering effects within the thick PDA cuboid microarrays (1.5 μm)[4]. Upon treatment with ACN both FL images and corresponding CPL performance could be partially recovered (Fig. 5a and Supplementary Fig. 26a), suggesting that FL and CPL

https://doi.org/10.1038/s41467-025-57649-1

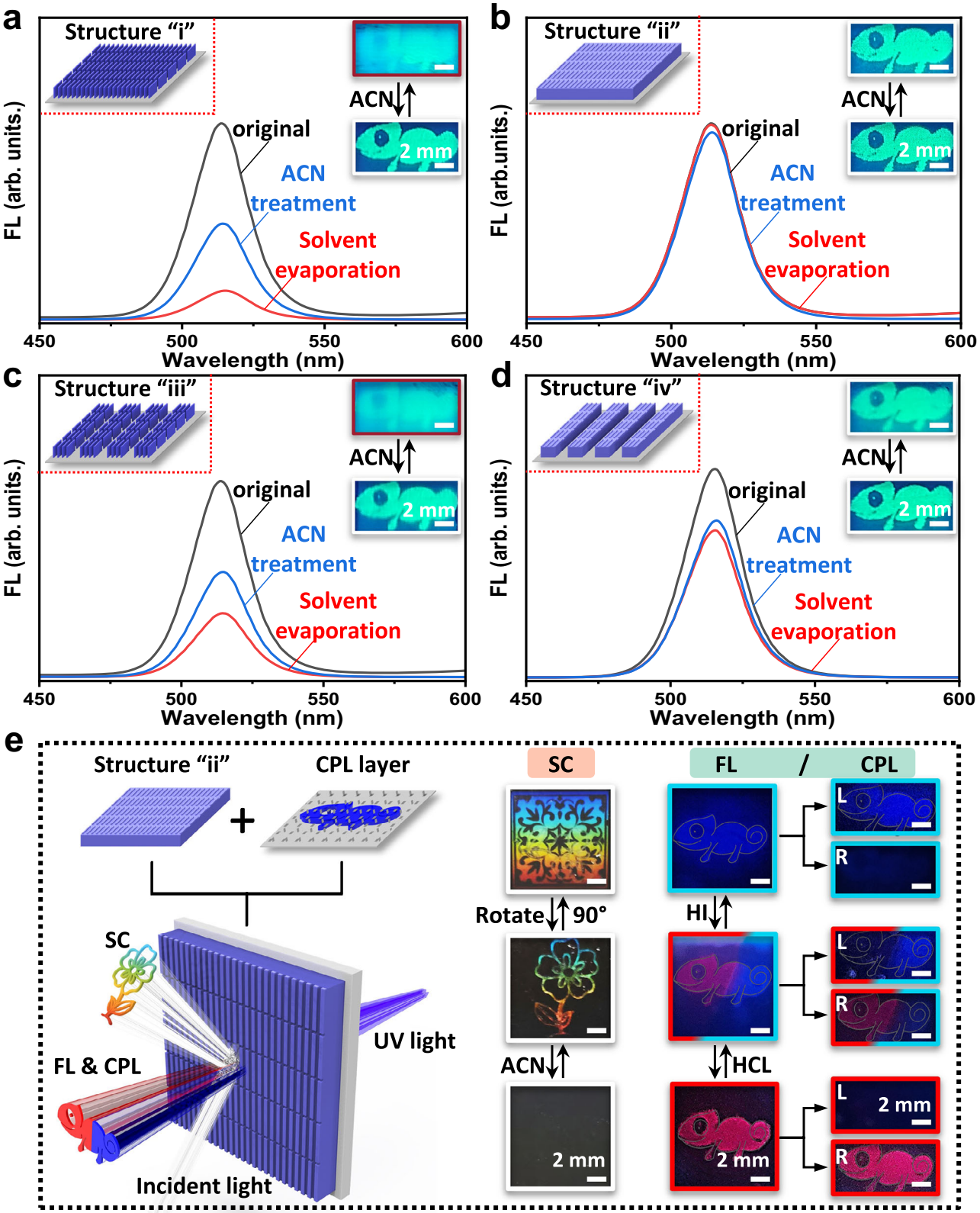

Fig. 5 | Combination of structural coloration, FL, and CPL. a–d FL spectra of hybrid films comprising chiral perovskite FL layer and PDA microarray with periodic structure "**i**" (**a**), "**ii**" (**b**), "**iii**" (**c**), or "**iv**" (**d**). The black, blue, and red curves represent the spectrum of pristine film, upon ACN treatment and after ACN removal, respectively. **e** Structural coloration, FL and CPL patterns can be modulated independently. Here structures "**ii**" is used as demo. Scale bar is 2 mm in all images.

patterns could be selectively concealed or exposed for reading by employing the structure "i" of PDA cuboid microarray as the upper layer. It should be noted here that independent modulation of SC and the FL/CPL signal could be easily achieved in the case of ACN treatment. However, the FL/CPL signal disappeared owing to strong diffraction and scattering effects within the thick PDA microarrays the upon removal of ACN. As for structure "ii", the upper PDA microarrays hardly affected the FL/CPL performance of the bottom fluorescent

https://doi.org/10.1038/s41467-025-57649-1

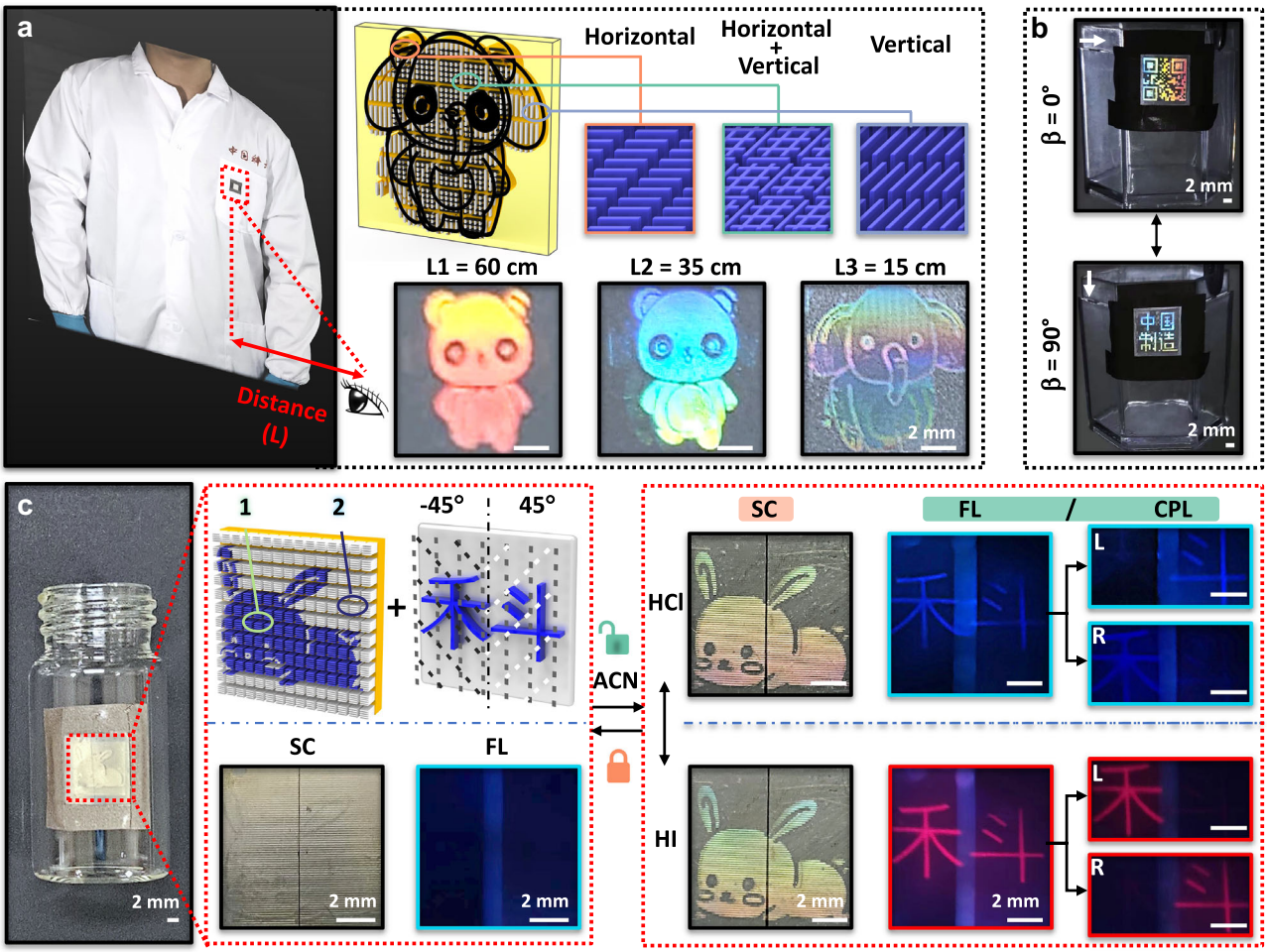

Fig. 6 | Potential applications of the multimodal dynamic anti-counterfeiting system. a A daylight scene where the color changes when observed from 60, 35, and 15 cm away. **b** Reversible patterns variation between "中国制造" and QR code pattern by changing the direction of incident light, *β*. **c** The structural coloration, fluorescence (including CPL) information could be concealed or exposed by ACN treatment. The fluorescence and CPL information could be further fine-tuned during the anion exchange process. The process is fully reversible. Scale bar is 2 mm.

layer (Fig. 5b), which should be ascribed to the low aspect ratio of PDA microarrays (80 nm) and their weak diffraction and scattering effects. Therefore, independent modulation of SC and the FL/CPL signal could be easily achieved. However, in the case of ACN treatment, SC disappeared owing to the easy penetration of ACN into the interior of the PDA microarray, resulting in the change in the refractive index contrast. In the case of structure "iii", the upper PDA microarrays hardly affected the FL/CPL performance in the case of ACN treatment (Fig. 5c), and independent modulation of SC and the FL/CPL signal could be easily achieved, similar as that of structure "i". As for structure "iv", the upper PDA microarrays hardly affected the FL/CPL performance (Fig. 5d), however, the SC was always concealed whether it was treated with ACN or not. Therefore, SC and FL/CPL information could be independently modulated, and selectively concealed or exposed for reading by rational design of PDA cuboid microarray as the upper layer. As mentioned above, the structure "ii" of PDA cuboid microarray as the upper layer would not interfere with the FL and CPL performance of chiral perovskite layer (Fig. 5b and Supplementary Fig. 26b), therefore, it was selected to construct multimodal dynamic information anti-counterfeiting system (Fig. 5e). By varying the incident light direction (angle *β*), the SC image can change from a "Chinese papercutting pattern" to a " flower" (Fig.5e), and the corresponding FL and CPL patterns in the same region is not interfered. Similarly, FL image and CPL patterns could be tuned through anion exchange process, without disturbing the SC images. Moreover, after treating the "chameleon" with HI in the designated region, it turned from blue to red (Fig. 5e). And a "chameleon" pattern consisting of blue and red FL could be observed by the naked eye. While using left- or right-handed CPF, only blue or red parts could be detected. In the case of the structure "iii", after removing ACN, SC patterns disappeared and FL and CPL intensities decreased greatly (Fig. 5c and Supplementary Fig. 26c), indicating that the information could be simultaneously concealed or exposed for reading. Finally, in the case of the structure "iv", after removing ACN, SC patterns disappeared while FL images and CPL performance were maintained (Fig. 5d and Supplementary Fig. 26d). Overall, it is clear that through periodic structural designs of the PDA cuboid microarrays, the SC information, FL signal, and even CPL patterns could be selectively concealed or exposed, allowing for multistage secure information encryption and programmable decryption.

In order to demonstrate the practical applications of the programmable SC, we further prepared anti-counterfeiting flexible labels on clothes where retroreflective vivid structural colors could be displayed depending on the different viewing conditions, making it especially useful in the field of smart advertisement displays. In a typical scene, a human is wearing a cloth decorated with an anti-counterfeiting flexible label (double periodic structure within the cuboid microarray: 10 μm in horizontal spacing and 1 μm in vertical spacing for the "panda" pattern, 1 μm in horizontal spacing and 10 μm in vertical spacing for the "elephant" pattern) and stands still (Fig. 6a),

when another person is approaching, the label can display different pattern depending on the distance between them. Specifically, one could see a colorful "panda" pattern at a distance of 35 to 60 cm, but an "elephant" pattern instead at distance of about 15 cm, as evidenced by the photographs shown in Fig. 6a. Also, depending on the viewing angle, one could see a dynamic switch between "panda" and "elephant" (Supplementary Fig. 27). As has been discussed above, this effect is related to the angle-dependent oscillations of the reflection peaks. Moreover, one can expect two completely different retroreflective SC patterns by varying the direction of the incident light (angle β), as depicted in Fig. 6b. When β is 0°, the QR code will be displayed and read by a smart phone, while when β is 90°, the words "中国制造" will be displayed instead. A similar phenomenon occurred by rotating the label that was coated to the lab vial (Supplementary Fig. 28), suggesting its practical applications in smart displays. Fundamentally, the effect behind is attributed to their inherent double periodic structure within the cuboid microarray, where the pattern "中国制造" with a periodic spacing of 1 μm was arranged vertically, while the pattern for the QR code was arranged horizontally with a periodic spacing of 1 μm.

Compared to single-mode patterns, dynamically encrypted multi-mode patterns have higher anti-counterfeiting security (Fig. 6c). Here a chiral perovskite FL layer with Chinese character "科" was prepared by screen printing with the ink of $CsPbCl_3$ NCs solution firstly, then a "rabbit" pattern with structure "iii" but featuring structure "iv" on the edges were integrated to fabricate multi-mode anti-counterfeiting labels. After removing ACN, no retroreflective SC patterns could be observed in both cases of structure "iii" and "iv", and corresponding FL and CPL information is also hidden by structure "iii". Therefore, neither SC patterns nor FL or CPL images could be observed, as shown in Fig. 6c and Supplementary Fig. 29. After treating with ACN, the "rabbit" pattern with structure "iii" could be observed clearly under daylight while the edge region with structure "iv" not. Upon illumination, a FL pattern of "科" appeared instead, suggesting that there is not much interference from the upper layer. Importantly, retroreflective SC as well as FL and CPL information could be reversibly modulated upon adding or removing ACN. In the FL mode, a blue "科" image could be observed. While in the case of CPL mode, only "斗" and "禾" blue images could be observed through left- and right-handed CPF respectively, as shown in Fig. 6c. Additionally, after treating with HI, $CsPbCl_3$ could be transformed to $CsPbI_3$ by anion exchange and red "科" image could be observed in FL mode, vice versa. While in the CPL mode, only "禾" and "斗" red images could be observed through left- and right-handed CPF respectively, as shown in Fig. 6c. The observed opposite CPL symbols originated from their opposite-handed CPL signal for $CsPbCl_3$ and $CsPbI_3$ (Fig. 4c, d). In the case of $CsPbBr_3$ NCs, a green "科" image could be observed in the FL mode. While in CPL mode, a similar green "科" image could be observed through left- or right-handed CPF (Supplementary Fig. 30), which should be ascribed to the relatively weak green CPL performance of the hybrid films. Overall, these multi-mode patterns feature unclonable cooperative stimuli-responsive capabilities and independent tunability and can be easily read under visible or UV light, thus providing an excellent platform with enhanced encryption capacity and security.

Discussion

Developing information encryption and anti-counterfeiting systems with dynamic multi-mode and multi-level characteristics is of great significance. At present, distinct optical channels, including SC and FL, have been widely used in information encryption systems. Extensive studies in this field are mainly focused on breaking through the limitations of orthogonal modulation. However, very little is known about the effect of the upper-layer microstructure on the underlying FL and CPL performance and the resulting dynamic modulation mechanism, which is crucial for the rational design of smart microstructure to actively manipulate light.

Based on these, we demonstrated a type of multimodal dynamic information encryption system that exploits interferometric retroreflection mechanism of the patterned photonic PDA microarrays. The combination of the reflected SC pattern produced by the photoprogrammable periodic orientation structural and the dynamically tunable transmitted FL and CPL patterns makes it possible to integrate several different optical information in the same device. By manipulating the aspect ratio of the 2D periodic structure of the upper diacetylene organogel microarrays, the orthogonal relationship between the SC pattern and the FL/CPL pattern could be accurately controlled.

Moreover, the SC information, including color gamut and patterns, could be tunned easily by varying the direction of incident light or by ACN treatment. The FL and CPL patterns (including color and handedness direction) could also be modulated by halogen anion exchange of the perovskite NCs. Switchable CPL signals (g_{lum}>1, reversible variation between left- and right-handed) allow for easy recognition even by the naked eye. Besides, the SC information, FL, and CPL patterns could be independently modulated without mutual interference during the dynamic regulation process and could be selectively concealed or exposed, allowing for multistage secure information encryption and programmable decryption. These optical properties would significantly enhance the encryption capacity, and also provide a straightforward approach for applications in smart display screens, smart coatings, indicators, and artistic decoration.

Methods

Materials

Silver nitrate ($AgNO_3$, ≥99.5%), cyclopentanone (>99.0%), and octadecene (ODE, 90%) were obtained from Sigma-Aldrich (St. Louis, MO, USA). PVP (polyvinylpyrrolidone K30, 99.8%), tert-butanol (≥99.5%), ethylene glycol (≥99.5%), oleic acid (≥99.5%), and all the other solvents were purchased from Sinopharm. Triethylamine (99.0%), 2,4-hexadiyn-1,6-diol (≥97%), acryloyl chloride (≥96%), Cs_2CO_3 (99.9%), $PbCl_2$ (99.99%), $PbBr_2$ (99%), PbI_2 (99.9%), 1-octadecanethiol (≥97%) and oleylamine (80–90%) were obtained from Aladdin. Ag nanowires (~40 nm in diameter and ~3 μm in length) were obtained according to previous report[37]. Perovskite NCs were prepared according to previous report[28,38] and 2,4-hexadiyn-1,6-diacrylate was synthesized according to the literature[30]. All the reagents and solvents were used as received without any further purification. Milli-Q water (18.2 MΩ cm) was used in all cases.

Measurements

^{1}H-NMR characterizations were recorded in chloroform-d on a Bruker Avance 400 MHz. All UV−Vis spectra were recorded on a Shimadzu UV-2550 PC spectrophotometer. Circular dichroism (CD) spectra were characterized by using JASCO CD spectrometer J-1500. Transmission electron microscopy (TEM) images were recorded on a JEOL-2000. SEM images were recorded on Sigma 300. Circularly polarized photoluminescence spectra of the samples were obtained by a JASCO CPL-300 spectrophotometer. Reflectance spectrum was characterized by using FLAME-T-VIS-NIR. Raman spectra were characterized by using LabRAM HR Evolution. Confocal microscopy image was obtained by Leica-DCM8.

Synthesis of Ag NWs

PVP (0.780 g) were added into glycerol (25 mL) in a 100 mL round bottle flask; then heating to 80 °C until PVP dissolved. After temperature dropped down to room temperature, silver nitrate (0.210 g) powder was added into the solution. Then glycerol (1.33 mL) and H_2O (67.0 μL) mixture containing NaCl (7.87 mg) were added into the flask. the solution temperature was raised from room temperature to 210 °C. When the temperature reached 210 °C, the heating was stopped and the temperature dropped back to room temperature slowly. Finally, H_2O was added into the solution in 1: 1 ratio, and then the mixture was

centrifuged at 8000 rpm. The as-obtained Ag NWs were washed by water and ethanol for three times, followed by hydrophobic treatment with 1-octadecanethiol for later use.

Synthesis of $CsPbX_3$ (X=Cl, Br, I) nanocrystals

Cs_2CO_3 (810 mg) was loaded into 100 mL 3-neck flask with octadecene (40 mL) and oleic acid (2.5 mL), dried at 120 °C for 1 h, and then heated under N_2 to 150 °C for 1 h.

ODE (50 mL) and PbX_2 (1.88 mmol) such as PbI_2 (870 mg), $PbBr_2$ (690 mg), $PbCl_2$ (520 mg) were loaded into 150 mL 3-neck flask and dried under vacuum at 120 °C for 1 h. Oleylamine (5 mL) and oleic acid (5 mL) were injected at 120 °C under N_2. After PbI_2 salt is completely dissolved, the temperature rises to 170 °C, and Cs-oleate solution (4 mL, 0.125 M in ODE) is quickly injected and after 5 s, the reaction mixture was cooled with the ice-water bath. The addition of tert-butanol (ODE: tert-butanol = 1:1 by volume) is helpful for complete precipitation. After centrifugation, the supernatant was discarded and the particles were redispersed in 10 mL hexane.

Synthesis of 2,4-hexadiyn-1,6-diacrylate

At room temperature, acrylyl chloride (2.47 g, 27.3 mmol) was added dropwise for 30 min to a solution of 2,4-hexadiene-1,6-diol (1.00 g, 9.10 mmol) and triethylamine (2.29 g, 22.7 mmol) in tetrahydrofuran (50 mL). Then the resulting solution mixture was stirred at 25 °C for 4 h. After vacuum concentration, the residue was dissolved in ethyl acetate and extracted three times with water, dried with $MgSO_4$, and filtered. The solvent was removed under vacuum and the residue was further purified by silica gel column chromatography (hexane/ethyl acetate = 5/1) to obtain the desired diacetylene monomer of 0.94 g (48%). ^{1}H-NMR (400 MHz, Chloroform-d) δ 6.47 (dd, J = 17.3, 1.4 Hz, 2H), 6.14 (dd, J = 17.3, 10.5 Hz, 2H), 5.92 (dd, J = 10.5, 1.3 Hz, 2H), 4.83 (s, 4H).

Fabrication of the chiral perovskite fluorescence layer

Firstly, 200 mg $CsPbX_3$ NCs solution (n-hexane, 40 mg/mL) was added into 400 mg of Sylgard 184 component B (curing agent) with stirring. After vacuum treatment at 40 °C for 1 h to remove solvent, the mixture was further added into 3.60 g of Sylgard 184 component A (silicone elastomer prepolymer). Then the fluorescent patterns, e.g., "butterfly", were fabricated on a flexible PET surface via a two-step screen printing technique. Finally, flexible polymeric FL layer could be prepared in a vacuum desiccator at 70 °C overnight.

Refer to previous literature[39,40], 3 mL as-prepared Ag NWs solution was spread dropwise onto the center of the container (ϕ = 15 cm) filled with EG surface with an injection rate of 20 mL/h. Immediately after the injection, a CTAC (Hexadecyl trimethyl ammonium chloride) aqueous solution (100 mM, 3 mL) was dropped at the center of the container to induce alignment of Ag NWs at the edge of liquid. The aligned Ag NWs were transferred onto the above hybrid $CsPbX_3$/PDMS film. After the solvent evaporated, the twisted-stacking Ag NWs was obtained onto the surface of the hybrid $CsPbX_3$/PDMS films by rotating the film clockwise or anticlockwise, generating high CPL ($g_{lum} > 1$).

Fabrication of multimodal optical materials combining structural coloration, fluorescence, and CPL

The precursor monomer (2 µL) was spread on the top of above chiral perovskite FL layer, after multistage irradiation with a mercury lamp through the combined photomask with the aligned grating, 2D photonic patterns with programmable SC could be fabricated on the chiral perovskite FL layer, producing multi-optical modal materials combining SC, FL, and CPL information.

Data availability

The authors declare that all relevant data supporting the findings of this study are available within this article and its supplementary information. Source data are provided with this paper. All data are available from the corresponding author upon request. Source data are provided with this paper.

References

1. Shen, Y., Le, X., Wu, Y. & Chen, T. Stimulus-responsive polymer materials toward multi-mode and multi-level information anti-counterfeiting: recent advances and future challenges. *Chem. Soc. Rev.* **53**, 606–623 (2024).
2. Zheng, Z. et al. Digital photoprogramming of liquid-crystal superstructures featuring intrinsic chiral photoswitches. *Nat. Photonics* **16**, 226 (2022).
3. Arppe, R. & Sorensen, T. J. Physical unclonable functions generated through chemical methods for anti-counterfeiting. *Nat. Rev. Chem.* **1**, 31 (2017).
4. Zhao, Y. et al. Crosstalk-free patterning of cooperative-thermoresponse images by the synergy of the AIEgen with the liquid crystal. *Angew. Chem. Int. Ed.* **59**, 10066–10072 (2020).
5. Ma, T. et al. Dynamic wrinkling pattern exhibiting tunable fluorescence for anticounterfeiting applications. *Nat. Commun.* **11**, 1811 (2020).
6. Xu, W.-C. et al. Designing rewritable dual-mode patterns using a stretchable photoresponsive polymer via orthogonal photopatterning. *Adv. Mater.* **34**, 2202150 (2022).
7. Qin, M. et al. Bioinspired hydrogel interferometer for adaptive coloration and chemical sensing. *Adv. Mater.* **30**, 1800468 (2018).
8. Kim, J. B., Chae, C., Han, S. H., Lee, S. Y. & Kim, S.-H. Direct writing of customized structural-color graphics with colloidal photonic inks. *Sci. Adv.* **7**, eabj8780 (2021).
9. Yang, W. et al. All-dielectric metasurface for high-performance structural color. *Nat. Commun.* **11**, 1864 (2020).
10. Miao, S., Wang, Y., Sun, L. & Zhao, Y. Freeze-derived heterogeneous structural color films. *Nat. Commun.* **13**, 4044 (2022).
11. Zheng, C., Tao, S. & Yang, B. Polymer-structure-induced room-temperature phosphorescence of carbon dot materials. *Small Struct.* **4**, 2200327 (2023).
12. Su, G. et al. Information-storage expansion enabled by a resilient aggregation-induced-emission-active nanocomposite hydrogel. *Adv. Mater.* **34**, 2207212 (2022).
13. Ou, Y. et al. Host differential sensitization toward color/lifetime-tuned lanthanide coordination polymers for optical multiplexing. *Angew. Chem. Int. Ed.* **59**, 23810–23816 (2020).
14. Sun, Y. et al. Dual-mode hydrogels with structural and fluorescent colors toward multistage secure information encryption. *Adv. Mater.* **36**, 2401589 (2024).
15. Gong, Z.-L. et al. Frontiers in circularly polarized luminescence: molecular design, self-assembly, nanomaterials, and applications. *Sci. China Chem.* **64**, 2060–2104 (2021).
16. Zhao, T., Han, J., Duan, P. & Liu, M. New perspectives to trigger and modulate circularly polarized luminescence of complex and aggregated systems: energy transfer, photon upconversion, charge transfer, and organic radical. *Acc. Chem. Res.* **53**, 1279–1292 (2020).
17. Sang, Y., Han, J., Zhao, T., Duan, P. & Liu, M. Circularly polarized luminescence in nanoassemblies: generation, amplification, and application. *Adv. Mater.* **32**, 1900110 (2020).
18. Huang, Z., Jiang, T., Wang, J., Ma, X. & Tian, H. Real-time visual monitoring of kinetically controlled self-assembly. *Angew. Chem. Int. Ed.* **60**, 2855–2860 (2021).
19. Liu, J. et al. What makes efficient circularly polarised luminescence in the condensed phase: aggregation-induced circular dichroism and light emission. *Chem. Sci.* **3**, 2737–2747 (2012).
20. Xia, Q. et al. Direct visualization of chiral amplification of chiral aggregation induced emission molecules in nematic liquid crystals. *Acs Nano* **15**, 4956–4966 (2021).

21. Li, Y., Yao, K., Chen, Y., Quan, Y. & Cheng, Y. Full-color and white circularly polarized luminescence promoted by liquid crystal self-assembly containing chiral naphthalimide dyes. *Adv. Opt. Mater.* **9**, 2100961 (2021).
22. Liu, S. J. et al. Circularly polarized perovskite luminescence with dissymmetry factor up to 1.9 by soft helix bilayer device. *Matter* **5**, 2319–2333 (2022).
23. Lan, R. et al. Orthogonally integrating programmable structural color and photo-rewritable fluorescence in hydrazone photoswitch-bonded cholesteric liquid crystalline network. *Angew. Chem. Int. Ed.* **61**, e202213915 (2022).
24. Huang, H. W. et al. Butterfly-inspired tri-state photonic crystal composite film for multilevel information encryption and anti-counterfeiting. *Adv. Mater.* **35**, 2211117 (2023).
25. Zhang, X. et al. A class of organic units featuring matrix-controlled color-tunable ultralong organic room temperature phosphorescence. *Adv. Sci.* **10**, 2206482 (2023).
26. Qin, L. et al. Geminate labels programmed by two-tone microdroplets combining structural and fluorescent color. *Nat. Commun.* **12**, 699 (2021).
27. Liu, C. et al. A photopatternable conjugated polymer with thermal-annealing-promoted interchain stacking for highly stable anti-counterfeiting materials. *Adv. Mater.* **35**, 2303120 (2023).
28. Sygletou, M., Kyriazi, M.-E., Kanaras, A. G. & Stratakis, E. Anion exchange in inorganic perovskite nanocrystal polymer composites. *Chem. Sci.* **9**, 8121–8126 (2018).
29. Zhao, C. et al. Scalable multistep imprinting of multiplexed optical anti-counterfeiting patterns with hierarchical structures. *Nano Lett.* **24**, 13638–13646 (2024).
30. Oh, J. et al. Dynamic multimodal holograms of conjugated organogels via dithering mask lithography. *Nat. Mater.* **20**, 385 (2021).
31. Rao, V. K., Teradal, N. L. & Jelinek, R. Polydiacetylene capacitive artificial nose. *ACS Appl. Mater. Interfaces* **11**, 4470–4479 (2019).
32. Geng, G. Z. et al. Height-gradiently-tunable nanostructure arrays by grayscale assembly nanofabrication for ultra-realistic imaging. *Laser Photonics Rev.* **17**, 2300073 (2023).
33. Nechifor, C. D., Postolache, M., Albu, R. M., Barzic, A. I. & Dorohoi, D. O. Induced birefringence of rubbed and stretched polyvinyl alcohol foils as alignment layers for nematic molecules. *Polym. Adv. Technol.* **30**, 2143–2152 (2019).
34. Han, Z. X., Wang, F., Sun, J. H., Wang, X. L. & Tang, Z. Y. Recent advances in ultrathin chiral metasurfaces by twisted stacking. *Adv. Mater.* **35**, 2206141 (2023).
35. Lv, J. W., Yang, X. K. & Tang, Z. Y. Rational design of all-inorganic assemblies with bright circularly polarized luminescence. *Adv. Mater.* **35**, 2209539 (2023).
36. Huang, H. et al. Dynamic passivation in perovskite quantum dots for specific ammonia detection at room temperature. *Small* **16**, 1904462 (2020).
37. Feng, Z. et al. Chiral biosensing at both interband transition and plasmonic extinction regions using twisted-stacked nanowire arrays. *Nanoscale* **14**, 10524–10530 (2022).
38. Protesescu, L. et al. Nanocrystals of cesium lead halide perovskites ($CsPbX_3$, X=Cl, Br, and I): Novel optoelectronic materials showing bright emission with wide color gamut. *Nano Lett.* **15**, 3692–3696 (2015).
39. Lv, J. et al. Gold nanowire chiral ultrathin films with ultrastrong and broadband optical activity. *Angew. Chem. Int. Ed.* **56**, 5055–5060 (2017).
40. Jung, D. et al. Highly conductive and elastic nanomembrane for skin electronics. *Science* **373**, 1022 (2021).

Acknowledgements

This study was supported by National Science and Technology Major Project (No. 2023ZD0120702, X.C.), the Strategic Priority Research Program of the Chinese Academy of Science (No. XDB0450302, G.Z.), National Natural Science Foundation of China (Nos. 22071233 and 52373122, G.Z.), Natural Science Foundation of Jiangsu Province, Major Project (No. BK20232012, X.C.), the open research fund of Suzhou Laboratory (No. SZLAB-1508–2024-ZD017, H.Z), Fundamental Research Funds for the Central Universities (No. WK2060000071, H.Z.), Youth Project of the Provincial Natural Science Foundation of Anhui (No. 2408085QB041, H.Z.) and AnHui Estone Materials Technology Co., Ltd. This work was partially carried out at the University of Science and Technology of China's Center for Micro and Nanoscale Research and Fabrication.

Author contributions

Z.F. and J.L. (J.L.L.) performed the experiments and analyzed the data. P.Y., X.X., D.W., J.L. (J.H.L.), C.Z., and J.L. (J.G.L.) discussed the results and have given approval to the final version of the manuscript descriptions. H.Z., X.C. and G.Z. conceived and designed the research and wrote the paper.

Competing interests

The authors declare no competing interests.

Additional information

Supplementary information The online version contains supplementary material available at https://doi.org/10.1038/s41467-025-57649-1.

Correspondence and requests for materials should be addressed to Hongli Zhang, Gang Zou or Xin Chen.

Peer review information *Nature Communications* thanks the anonymous reviewers for their contribution to the peer review of this work. A peer review file is available.